

# Unsupervised and self-adaptative techniques for cross-domain person re-identification

Gabriel Bertocco, Fernanda Andaló, *Member, IEEE*,  
and Anderson Rocha, *Senior Member, IEEE*

**Abstract**—Person Re-Identification (ReID) across non-overlapping cameras is a challenging task and most works in the prior art rely on supervised feature learning from a labeled dataset to match the same person in different views. However, it demands the time-consuming task of labeling the acquired data, prohibiting its fast deployment in forensic scenarios. Unsupervised Domain Adaptation (UDA) emerges as a promising alternative, as it performs feature adaptation from a model trained on a source to a target domain without identity-label annotation. However, most UDA-based methods rely upon a complex loss function with several hyper-parameters, which hinders the generalization to different scenarios. Moreover, as UDA depends on the translation between domains, it is important to select the most reliable data from the unseen domain, avoiding error propagation caused by noisy examples on the target data — an often overlooked problem. In this sense, we propose a novel UDA-based ReID method that optimizes a simple loss function with only one hyper-parameter and takes advantage of triplets of samples created by a new offline strategy based on the diversity of cameras within a cluster. This new strategy adapts and regularizes the model, avoiding overfitting on the target domain. We also introduce a new self-ensembling strategy, in which weights from different iterations are aggregated to create a final model combining knowledge from distinct moments of the adaptation. For evaluation, we consider three well-known deep learning architectures and combine them for final decision-making. The proposed method does not use person re-ranking nor any label on the target domain, and outperforms the state of the art, with a much simpler setup, on the Market to Duke, the challenging Market1501 to MSMT17, and Duke to MSMT17 adaptation scenarios.

**Index Terms**—Person Re-Identification, Unsupervised Learning, Deep Learning, Curriculum Learning, Network Ensemble.

## I. INTRODUCTION

**P**ERSON Re-Identification (ReID) has gained increasing attention in the last years in the Computer Vision and Forensic Science communities, due to its broad range of applications in person tracking, crime investigation, and surveillance. One of the main goals when dealing with forensic problems is to answer “who took part in an event?”. Person ReID comprises the primary techniques to find possible people, or groups of people, involved in an event and to, ultimately, propose candidate suspects for further investigation [1].

Person ReID aims to match the same person in different non-overlapping views in a camera system. Thanks to the considerable discrimination power given by deep learning, recent works [2], [3], [4], [5], [6] consider supervised feature learning on a labeled source dataset, which yields high values of mean Average Precision (mAP) and top Ranking accuracy.

However, the labeling of massive datasets demanded by deep learning is time-consuming and error-prone, especially when targeting forensic applications. In this context, Unsupervised Domain Adaptation (UDA) aims to adapt a model trained on a source dataset to a target domain without the need for identity information of the target samples. Most ReID methods that follow this approach are based on label proposing, in which feature vectors of target images are extracted and clustered. Upon supervised training, these clusters receive pseudo-labels to be adapted to the target domain.

Several works [7], [8], [9], [10], [11] apply the pseudo-labeling principle by developing different ways to propose and refine clusters on the target domain. The aim is to alleviate noisy labels, which can harm feature learning. The method we introduce herein follows this trend, but we consider a more general clustering algorithm differently from previous work, which can relax the criteria to select data points, allowing clusters with arbitrary densities in feature space. By not forcing all clusters to have the same complexity, we can utilize the density information to filter relevant data points better.

As we are dealing with data from an unknown target domain, clusters can have different degrees of reliability, i.e., contain different quantities of noisy labels. We need to select the most reliable clusters to optimize the model at each iteration of the clustering process. The generated model must also be camera-invariant to generate the same feature representation for an identity, regardless of the camera point of view. Based on these observations, we hypothesize that clusters more diverse in terms of camera representation might be more reliable to optimize the model. Suppose a cluster contains images of the same identity seen from two or more cameras. This means that the model can embed these images close to each other in the feature space, overcoming differences in illumination, pose, occlusion, among others, which are inherently present in different camera vantage points.

We argue that the greater the number of different cameras in a cluster, the more reliable this cluster to optimize the model. Following this idea, we propose a new way to create triplets of samples in an offline manner. For each camera represented in a cluster, we select one sample as an anchor and two others as positive and negative examples. As a positive example, we

Gabriel Bertocco is a Ph.D. student at the Institute of Computing, University of Campinas, Brazil

Fernanda Andaló is a researcher associated to the Institute of Computing, University of Campinas, Brazil

Anderson Rocha is an Associate Professor at the Institute of Computing, University of Campinas, Brazil

Manuscript received on March 31st, 2021; revised on XX 2021.

select a sample from one of the other represented cameras, while the negative example is a sample from a different cluster but with the same camera as the anchor. Consequently, the greater the number of cameras in a cluster, the more diverse the triplets to train the model. With this approach, we give more importance to the more reliable clusters, regularize the model, and alleviate the dependency on hyper-parameters by using a single-term and single-hyper-parameter triplet loss function. This brings robustness and generability to the final model, easing its adaptation to different scenarios.

Another important observation is that, at different points of the adaptation from a source to a target domain, the model holds different levels of knowledge as different portions of the target data are considered each time. We argue that the model has complementary knowledge in different iterations during training, and we propose a self-ensembling strategy to summarize the knowledge from different iterations into a unique final model.

Finally, based on recent advances in ensemble-based methods for ReID [12], [13], we propose to combine the knowledge acquired by different architectures. Unlike prior work, we avoid complex training stages by simply assembling the results from different architectures only during evaluation time.

To summarize, the key contributions of our work are:

- A new approach to creating diverse triplets based on the variety of cameras represented in a cluster. The greater the number of cameras in a cluster, the greater the number of cross-camera pair combinations used to train the model. This helps the model be camera-invariant and more robust in generating the same person's features from different perspectives. It allows us to leverage a single-term and single-hyper-parameter triplet loss function to be optimized.
- A novel self-ensembling fusion method, which enables the final model to summarize the complementary knowledge acquired during training. This method relies upon the knowledge hold by the model in different checkpoints of the adaptation process.
- A novel ensemble technique to take advantage of the complementarity of different backbones trained independently. Instead of applying the typical knowledge distilling [14] or co-teaching [15], [16] methods, which add complexity to the training process, we propose the use of an ensemble-based prediction.

## II. RELATED WORK

Several works have been proposed to address Unsupervised Domain Adaptation for Person Re-Identification. They can be roughly divided into three categories: generative, attribute alignment, and label proposing methods.

### A. Generative Methods

ReID generative methods aim to synthesize data by translating images from a source to a target domain. Once data from the source dataset is labeled, the translated images on the target context receive the same labels as the corresponding original images. The main idea is to transfer low-level and mid-level

characteristics from the target domain, such as background, illumination, resolution, and, in some cases, even clothing, to the images in the source domain. These methods create a fully synthetic dataset of labeled images with the same conditions as the target domain. They apply supervised training to adapt the model. Some works in this category are SPGAN [17], PTGAN [18], AT-Net [19], CR-GAN [20], PDA-Net [21], and HHL [22]. Besides transferring the characteristics from source to target domain (and vice-versa) for image-level generation, DG-Net++ [23] also applies label proposing through clustering. The final loss is the aggregation of the GAN-based loss function to generate images, along with the classification loss defined for the proposed labels. By doing this, they perform the disentangling and adaptation of the features on the target domain manifold.

### B. Attribute Alignment Methods

These methods seek to align common attributes in both domains to ease the transfer of knowledge from source to target. Such features can be clothes, objects dressed by people (backpacks, hats, shoes), and other soft-biometric attributes that might be common in both domains. Those works align mid-level features and enable the whole model to learn higher semantic features on the target domain. Works such as TJ-AIDL [24] consider a fixed set of attributes (23 to 27 attributes). However, source and target domains can have substantial context differences, leading to potentially different attributes. For example, the source could be recorded in an airport while the target domain comprises a shopping center. To obtain a better generalization, in [25], the authors propose the Multi-task Mid-level Feature Alignment (MMFA) technique to enable the method to learn attributes from both domains and align them for a better generalization on the target domain. Other methods, such as UCDA [26] and CASCL [27], aim to align attributes by considering images from different cameras on the target dataset.

### C. Label Proposing Methods

Methods in this category predict possible labels for the unlabeled target domain by leveraging clustering methods (K-means [28], DBSCAN [29], among others). Once the target data is pseudo-labeled, models are trained to learn discriminative features on the new domain. PUL [7] applies the Curriculum Learning technique to adapt a model learned on a source domain to a target domain. However, as K-means is applied to cluster the features, it is not possible to account for camera variability. As K-means generates only convex clusters, it cannot find more complex cluster structures, hindering the performance. UDAP [8] and ISSDA-ReID [30] utilize DBSCAN as the clustering algorithm along with labeling refinement. SSG [9] also applies DBSCAN to cluster features extracted from the whole, upper, and low body parts of identities of interest.

ECN [31], ECN-GPP [32], MMCL [33] and Dual-Refinement [34] make use of a memory bank to store features, which is updated along the training to avoid the direct use of features generated by the model in further iterations. The

authors aim to avoid propagating noisy labels to future training steps, contributing to keep and increase the discrimination of features during training.

PAST [10] applies HDBSCAN [35] as the clustering method, which is similar to OPTICS [36] — the algorithm of choice in our work. However, the memory complexity of OPTICS is  $O(n)$ , while for HDBSCAN is  $O(n^2)$ , making our model more memory efficient in the clustering stage.

MMT [12], MEB-Net [13], ACT [37], SSKD [38] and ABMT [16] are ensemble-based methods. They consider two or more networks and leverage mutual teaching by sharing one network's outputs with the others, making the whole system more discriminative on the target domain. However, training models in a mutual-teaching regime brings complexity in memory and generally to the training process. Besides that, noisy labels can be propagated to other ensemble models, hindering the training process. Nonetheless, ensemble-based learning provides the best performance among state-of-art methods. We propose the use of ensembles only during inference to simultaneously eliminate the complexity added to the training, still taking advantage of knowledge complementary between the models.

Our work is also based on Curriculum Learning with Diversity [39], which is a curriculum learning schema whereby the model starts learning with easier examples, i.e., samples that are correctly classified with a high score to their respective ground-truth classes early in training. However, in a multi-class problem, one of the classes might have more examples correctly classified early on training, making it easier than the other classes. In Curriculum Learning with Diversity, the model is designed to select the most confident samples (easier samples) from the easier classes, including some examples from the harder ones. In this way, it enables the model to learn in an easy-to-hard manner, avoiding local minima and allowing better generalization.

Even though some recent work achieved competitive performances, they show some limitations that we aim to address in our work. Generative methods bring complexity by considering GANs to translate images from a domain to the other. Attribute Alignment methods only tackle the alignment of low and mid-level features. Methods in both categories need images from source and target domains during adaptation. The last Label Proposing methods consider mutual-learning or co-teaching, which brings complexity to the training stage.

Differently from these approaches, we do not have or assume label identity on the target domain, by using a new diversity learning scheme and generating triplets proportional to the diversity of points-of-view on each cluster. And as we train the whole model, the method also learns high-level features on the target domain. Furthermore, we simplify the training process by considering one backbone at a time, without mutual information exchange during adaptation. We apply model ensembling for inference, after the training process.

### III. PROPOSED METHOD

Our approach to Person ReID comprises two phases: training and inference. Training is shown in Figure 1. We independently optimize  $n_{model}$  different backbones to adapt the model

to the target domain. This phase is divided into five main stages that are performed iteratively: feature extraction from all data; clustering; cluster selection; cross-camera triplet creation and fine-tuning; feature extraction from pseudo-labeled data.

After training, we perform the proposed self-ensembling phase to summarize the training parameters in a single final model based on the weighted average of model parameters from each different checkpoint. We perform this step for each backbone independently and, in the end, we have  $n_{model}$  self-ensembled models.

During inference, for a pair query/gallery image, we calculate the distance between them considering feature vectors extracted by each of the  $n_{model}$ . Hence, for each query/gallery pair, we have  $n_{model}$  distances, one for each of the trained models. We then apply our last ensemble technique: the  $n_{model}$  distances are averaged to obtain a final distance. Finally, based on this final distance, we take the label of the closest gallery image as the query label.

#### A. Training Stages 1 and 2: Feature Extraction from all data and Clustering

Let  $D^s = \{(x_i^s, y_i^s)\}_{i=1}^{N_s}$  be a labeled dataset representing the source domain, formed by  $N_s$  images  $x_i^s$  and their respective identity labels  $y_i^s$ ; and let  $D^t = \{(x_i^t)\}_{i=1}^{N_t}$  be an unlabeled target dataset representing the target domain, formed by  $N_t$  images  $x_i^t$ . Before applying the proposed pipeline, we firstly train a model  $M$  in a supervised way, with source dataset  $D^s$  and its labels. After training, assuming source dataset  $D^s$  is not available anymore, we perform transfer learning, updating  $M$  to the target domain, only considering samples from unlabeled target dataset  $D^t$ .

With model  $M$  trained on  $D^s$ , we first extract all feature vectors from images in  $D^t$  and create a new set of feature vectors  $\{M(x_i^t)\}_{i=1}^{N_t}$ . We remove possible duplicates by checking if there is a replacement from one of them, which might be caused by duplicate images on target data. The remaining feature vectors are L2-normalized to embed them into a unit hypersphere. The normalized feature vectors are clustered using the OPTICS algorithm to obtain pseudo labels.

The OPTICS algorithm [36] leverages the principle of dense neighborhood, similarly to DBSCAN [29]. DBSCAN defines the neighborhood of a sample as being formed by its closest feature vectors, with distances lower than a predefined threshold. Based on these neighborhoods, clusters are created, and samples not assigned to any cluster are considered outliers. If the threshold changes, other clusters are discovered, current clusters can be split or even combined to create new ones. In other words, if we change the threshold, other clusters might appear, creating a different label proposing for the samples. However, clusters that emerge from real labels often have different distributions and densities, indicating that a generally fixed threshold might not be sufficient to detect them. In this sense, OPTICS relaxes DBSCAN by ordering feature vectors in a manifold based on the distances between them, which allows the construction of a *reachability plot*. Probable clusters with different densities are revealed as valleys in this plot and can be detected by their steepness. We are more likely

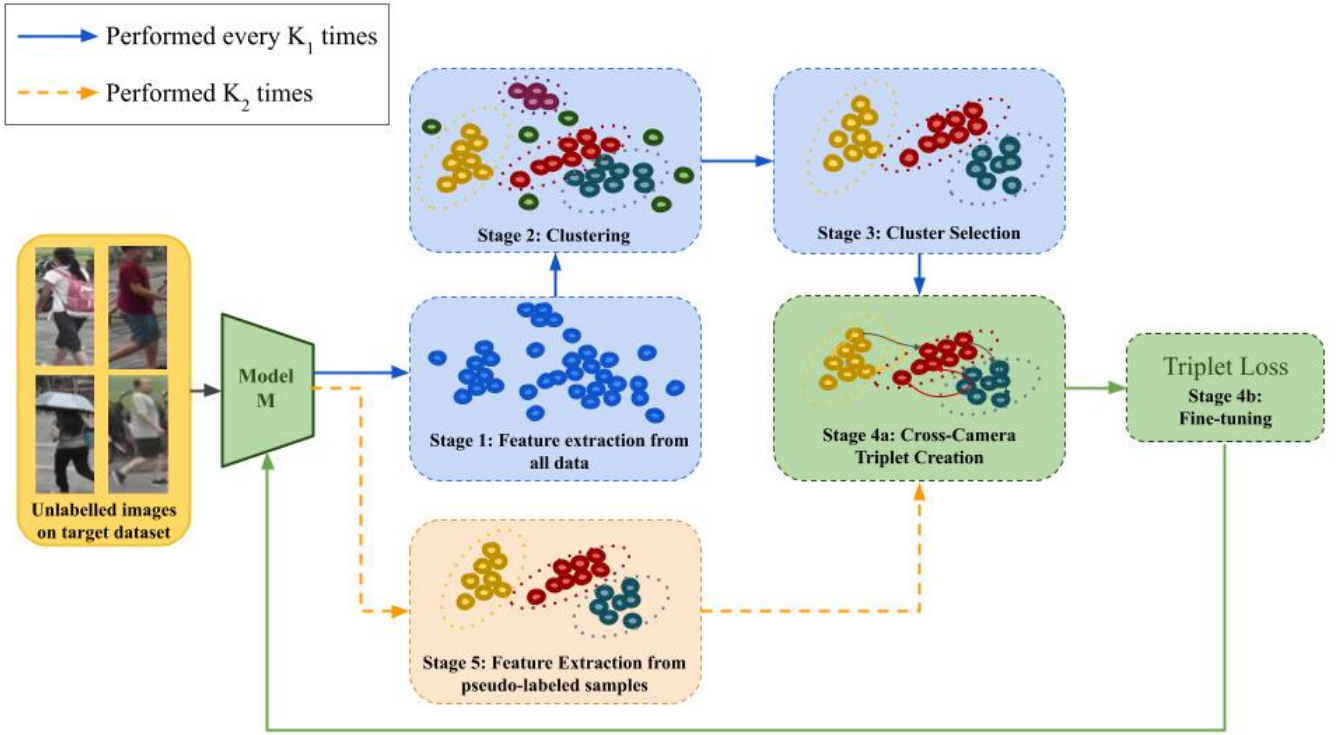


Fig. 1. Overview of the training phase to adapt the model to a target domain. Our model needs only target images during adaptation and does not rely on any target label information. The pipeline has two flows: the blue flow is executed every  $K_1$  times and the orange flow is executed  $K_2$  times. Steps in green are shared by both flows. Initially, in Stage 1, we extract feature vectors for each training image in the target domain using model  $M$ , and cluster them using the OPTICS algorithm in Stage 2. Afterward, we perform cluster selection in Stage 3, removing outliers and clusters with only one camera type. Then, triplets are created based on each cluster's diversity in Stage 4a and used to train the model in Stage 4b. These steps are denoted by the blue flow in which the Clustering and Cluster Selection are performed. Instead of going back to Stage 1, the method follows to the orange flow. In Stage 5 we extract feature vectors of the samples selected in Stage 3 and the method continues to Stage 4a and 4b again. The blue flow marks an iteration, while the orange flow is called an epoch. Therefore, in each iteration, we have  $K_2$  epochs.

to propose labels closer to real label distribution on the target data with this formulation.

### B. Training Stage 3: Cluster Selection

After the first and second stages, feature vectors are either assigned to a cluster or considered as outliers. As people can be captured by one or more cameras in a ReID system, the produced clusters are naturally formed by samples acquired by different devices. We hypothesize that clusters with samples acquired by two or more cameras are more reliable than clusters with only one camera type.

If an identity is well described by model  $M$ , its feature vectors should be closer in the feature space regardless of the camera type. Therefore, clusters with only one camera might be created due to bias to a particular device or viewpoint, and different identities captured by the same camera can be assigned to the same cluster because of this bias. Besides, if a feature vector is predicted as an outlier by the clustering algorithm, it means that it does not have a good description of its image identity to be assigned to a cluster.

Based on these observations and for optimization purposes, we filter the feature vectors by discarding outliers and clusters with a single camera type. Figure 1 depicts this process, from Stage 2 to Stage 3, in which the outlier samples (green

points) and clusters with only one camera (magenta points) are removed from the feature space.

The remaining clusters (the ones with two or more cameras) are considered reliable to fine-tune model  $M$ . Furthermore, different clusters have different degrees of reliability based on the number of represented cameras. If images captured by several cameras form a cluster, it means model  $M$  is capable of embedding, in the feature space, samples of the corresponding identity captured by all of these cameras, eliminating point-of-view bias. In contrast, the lesser the number of images from different points of view, the more complex the identity definition. In this sense, we propose a new approach of creating cross-camera triplets of samples to optimize the model by emphasizing cluster diversity and forcing samples of the same identity to be closer in the feature space regardless of their acquisition camera.

### C. Training Stage 4: Cross-Camera Triplet Creation and Fine-tuning

Figure 2 shows the triplet creation process. A triplet is formed by an anchor, a positive, and a negative sample. During optimization, the idea is that the distance from the anchor to the positive sample is minimized while the distance from the anchor to the negative sample is maximized. Ideally, both positive and negative samples should be hard-to-classify

examples for the current model  $M$  as easy examples do not bring diversity to the learning process.

We initially select, as the anchor, one random sample in cluster  $c$  captured by camera  $cam_j$ . For each camera  $cam_k \neq cam_j$  in cluster  $c$ , we sort all feature vectors from camera  $cam_k$  based on their distance to the anchor. The positive sample is then selected as being the median feature vector. The median is considered instead of the farthest sample (which would be the hardest example) to avoid selecting a noisy example. We do not choose an easy example (which would be the closest one) to avoid slowing down the model convergence or even getting stuck on a local minimum. To select the negative sample, we first sort all feature vectors from camera  $cam_j$ , but belonging to other clusters  $\neq c$ , based on their distance to the anchor. We pick the closest feature vector that has not been assigned yet to a triplet as the negative sample. In this way, we avoid selecting the same negative sample, which brings diversity to the triplets and alleviates the harmful impact if one of the negative samples shares the anchor's same real identity.

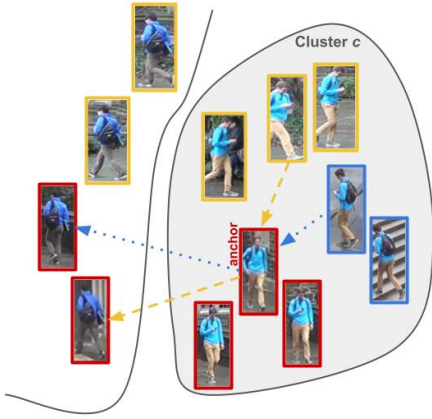


Fig. 2. Cross-Camera Triplet Creation. For each selected cluster, we have at least two cameras. Suppose the represented cluster  $c$  has images from three cameras (represented with red, blue, and yellow contours). For each camera, we select  $m$  anchors and, for each anchor, we create triplets with a positive sample from other cameras in the same cluster and a negative sample with the same camera in other clusters. For instance, for camera red, we select an anchor and we sort, based on the distance, all feature vectors from cameras yellow and blue. Then we select the median feature vector from each one (represented by the arrows coming to the anchor). To select the negative sample, we sort all feature vectors from the same camera but from a cluster  $\neq c$  and we choose the closest and not previously selected sample. For the triplet with yellow median sample as positive, we select as negative the closest sample to red anchor from another cluster (represented by the yellow arrow leaving the anchor). For the triplet with blue median sample as positive, we select the second closest feature vector to the red anchor from another cluster (since the first closest has already been picked). This explanation assumes  $m = 1$  and is repeated for cameras yellow and blue.

For a cluster  $c_i$  with  $n_i$  cameras, we generate a total of  $n_i - 1$  triplets with the same anchor. If we select  $m$  anchors for one camera in  $c_i$ , a total of  $m(n_i - 1)$  triplets are created. Considering that this process is repeated for each camera in  $c_i$ , we have a total of  $n_i m(n_i - 1)$  triplets for cluster  $c_i$ . Note that the triplets are created in an offline manner. The offline creation enables us to choose triplets considering a global view of the target data instead of creating them in a batch, which

would bring a limited view of the target feature space.

The number  $m$  of anchors of a camera is defined as the same for all clusters. Consequently, the number of triplets generated for a cluster  $c_i$  is  $\mathcal{O}(n_i^2)$ . The greater the diversity of cameras in a cluster, the greater its representativeness on the triplets. This emphasizes the clusters with more camera diversity during training, making the model learn from easy-to-hard identities and be more robust to different viewpoints. In our experiments we set  $m = 2$  for all adaptation scenarios.

Due to this new approach of creating cross-camera triplets, we can optimize the model by using the triplet loss [40] without the need for weight decay or any other regularization term and hyper-parameters. This also suggests that cross-camera triplets help to regularize the model during training.

After creating the triplets in an offline manner, we optimize the model using the standard triplet loss function:

$$L = \frac{1}{|B|} \sum_{(x_a, x_p, x_n) \in B} [d(x_a, x_p) - d(x_a, x_n) + \alpha]_+, \quad (1)$$

where  $B$  is a batch of triplets,  $x_a$  is the anchor,  $x_p$  is the positive sample and  $x_n$  is the negative one.  $\alpha$  is the margin that is set to 0.3 and  $[\cdot]_+$  is the  $\max(0, \cdot)$  function. This is illustrated in Figure 1, Stage 4b.

#### D. Stage 5: Feature Extraction from Pseudo-Labeled Samples

This stage is part of the orange flow performed after Fine-tuning (Stage 4b). The main idea is to keep the pseudo-labeled clusters from Stage 3, recreating a new set of triplets based on the new distances between samples after the model update in Stage 4b, bringing more diversity to the training phase. To do so, we extract feature vectors only for samples of the pseudo-labeled clusters selected in Stage 3. The orange flow is performed  $K_2$  times and a complete cycle defines an epoch. The blue flow is performed every  $K_1$  times, and a complete cycle defines an iteration. Therefore, in each iteration, we have  $K_2$  epochs. This concludes the training phase.

Differently from the five best state-of-the-art methods proposed in the prior art (DG-Net++, MEB-Net, Dual-Refinement, SSKD, and ABMT), our solution is trained with a single-term loss and only one hyper-parameter in the loss function. Even the weight decay has been removed, as the proposed method can already calibrate the gradient to avoid overfitting, as we show in Section IV. Moreover, prior work perform clustering on the training phase through k-reciprocal Encoding [41], which is a more robust distance metric than Euclidean distance. However, it has a higher computational footprint, as it is necessary to check the neighborhood of each sample whenever distances are calculated. For training simplicity, we opt for standard Euclidean distance to cluster the feature vectors. However, as k-reciprocal encoding gives the model higher discrimination, we adopt it during inference time. Therefore, different from previous works, we calculate k-reciprocal encoding only once during inference.

#### E. Self-ensembling

Our last contribution relies upon the curriculum learning theory. In different iterations of the training phase, different



amounts of reliable data are considered from the target domain, as shown in Section IV. This property leads us to hypothesize that knowledge obtained at different iterations is complementary. Therefore, we propose to summarize knowledge from different moments of the optimization in a unique final model. However, as the model discrimination ability increases as more iterations are performed (the model is able to learn from more data), we propose to combine the model weights of different iterations by weighting their importance with the amount of reliable data used in the corresponding iteration. We perform this weighted average of the model parameters as:

$$\theta_{final} = \frac{\sum_{p \in P} p_i \cdot \theta_i}{\sum_{p \in P} p_i}, \quad (2)$$

where  $\theta_i$  represents the model parameters after the  $i$ -th iteration and  $p_i$  is the weight assigned to  $\theta_i$ . Weight  $p_i$  is obtained based on the reliability of the target domain; if more data from the target domain is considered in an iteration, it means that the model is more confident, and then it can have more discrimination power on the target domain. Hence,  $p_i$  is equal to the percentage of reliable target data in the  $i$ -th iteration. Consequently, a model that takes more data from the target to train will have a higher weight  $p_i$ . Self-Ensembling is illustrated in Figure 3. Note that we are directly dealing with the model's learned parameters and creating a new one by averaging the weights.

We end up with a single model containing a combination of knowledge from different adaptation moments, which significantly boosts performance, as we show in Section V.

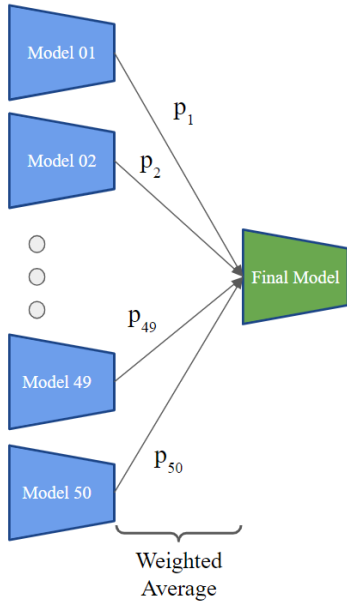


Fig. 3. Self-Ensembling scheme after training. Different amounts of the target data (with no label information whatsoever) are used to fine-tune the model during the adaptation process. Different models are created along the adaptation and they can be complementary. We create a new final model by weight averaging the models' parameters from different iterations. Weight  $p_i$  is based on the amount of reliable data from the target domain on the  $i$ -th iteration. We end up with a single model encoding knowledge from different moments of the adaptation.

#### F. Ensemble-based prediction

After training and performing the self-ensemble fusion, we have a single model adapted from the source to the target domain. However, due to the high performance of ensemble-based methods in recent ReID literature [12], [13], as a last measure, we leverage a combination of  $n_{model}$  different architectures to make a final prediction considering even more learned knowledge, which improves performance on the target dataset. We apply the ensemble technique only for inference, different from [12], [13] that leverage a mutual-teaching regime on training time. In turn, we avoid bringing complexity to the training but still take advantage of the complementarity from different architectures during inference.

To perform the ensemble-based prediction, we first calculate the feature distance of the query to each image on gallery for each of the  $n_{model}$  final models. Let  $f_k(x) = M_k(x)$  be the L2-normalized feature vector of image  $x$  obtained with model  $M_k$  and  $d(f_k(q), f_k(g_i))$  be the distance between the feature vectors of the query  $q$  and of the  $i$ -th image gallery  $g_i$  extracted using the  $k$ -th model on ensemble. The final distance between query  $q$  and gallery image  $g_i$  is given by:

$$d_{final}(q, g_i) = \frac{1}{K} \sum_{k=1}^K d(f_k(q), f_k(g_i)), \quad (3)$$

where  $K$  is the number of models in the ensemble. In this way, we can incorporate knowledge from different models encoded as the distance between two feature vectors. After obtaining the distance between query  $q$  and all images in the gallery, we take the label of the closest gallery image as the query label.

## IV. EXPERIMENTS AND RESULTS

This section presents the datasets we adopt in this work and compares the proposed method with the prior art with a comprehensive set of experiments considering different, and challenging, source/target domains.

#### A. Datasets

To validate our pipeline, we used three large-scale benchmark datasets present on Re-ID literature:

- Market1501 [42]: It has a total of 12,936 images of 751 identities in the training set and 19,732 images in the testing set. The testing set is still divided into 3,368 images for the query set and 15,913 images for the gallery set. Following previous prior work, we removed the “junk” images from the gallery set, so 451 images are discarded. This dataset has a total of six non-overlapping cameras. Each identity is captured by at least two cameras.
- DukeMTMC-ReID [43]: It has 16,522 images of 702 identities in the training set and 19,889 images in the testing set. The testing set is also divided into 2,228 query images and 17,661 gallery images of other 702 identities. The dataset has a total of eight cameras. Each identity is captured by at least two cameras.
- MSMT17 [18]: It is the most challenging ReID dataset present in the prior art. It comprises 32,621 images of 1,401 identities in the training set and 93,820 images

of 3,060 identities in the testing set. Similar to the two previous ones, the testing set is divided into 11,659 images for a query set and 82,161 images for gallery set. It comprises 15 cameras recorded in three periods of the day (morning, afternoon, and noon) on four different days. Besides, from the 15 cameras, 12 are outdoor cameras, and three are indoor cameras. Each identity is captured by at least two cameras.

As done in previous work in the literature, we remove from the gallery images with the same identity and camera of the query to assess the model performance in a cross-camera matching. Feature vectors are L2-normalized before calculating distances. For evaluation, we calculate the Cumulative Matching Curve (CMC), from which we report Rank-1 (R1), Rank-5 (R5), and Rank-10 (R10), and mean Average Precision (mAP).

### B. Implementation details

In terms of deep-learning architectures, we adopt ResNet50 [44], OSNet [4], and DenseNet121 [45], i.e.  $n_{models} = 3$ , all of them pre-trained on ImageNet [46]. To test them on an adaptation scenario, we choose one of the datasets as the source and another as the target domain. We train the backbone over the source domain and leverage the adaptation pipeline over the target domain. We consider, in our experiments, as source domain Market1501 and DukeMTMC-ReID and leave MSMT17 only as the target dataset (the hardest one in the prior art). This way, we have four possible adaptation scenarios: Market  $\rightarrow$  Duke, Duke  $\rightarrow$  Market, Market  $\rightarrow$  MSMT17, and Duke  $\rightarrow$  MSMT17. We keep those scenarios (without putting MSMT17 as a source) to have a fair comparison with state-of-the-art works. Besides, when we consider MSMT17 as the target dataset, we have the most challenging scenario: we train backbones on simpler datasets (Market and Duke) and adapt their knowledge to a harder dataset with almost the double number of cameras with many more identities recorded in different moments of the day and of the year. This enables us to test the generalization of our method in adaptation scenarios where source and target domain have substantial differences in the number of identities, camera recording conditions, and environment.

We used the code available at [47] to train OSNet and at [13] to train ResNet50 and DenseNet121 over the source domains. Our source-code is based on PyTorch [48] and will be freely available at GitHub upon acceptance of this paper.

After training, we remove the last classification layer from all backbones and use the last layer's output as our feature embedding. We trained our pipeline using the three backbones independently in all scenarios of adaptation. Considering the flows depicted in Figure 1, we perform  $K_1 = 50$  cycles of the blue flow (50 iterations), and, in each one, we perform  $K_2 = 5$  cycles of the orange flow (5 epochs). We consider Adam [49] as the network optimizer and set the learning rate to 0.0001 in the first 30 iterations. After the 30<sup>th</sup> iteration, we divided it by ten and kept it unchanged until reaching the maximum number of iterations. Weight decay is set to zero since, as we show in our experiments, our proposed Cross-Camera Triplet Creation

can regularize the model without adding any hyper-parameter to calibrate the regularization. The triplet batch size was set to 30; in each epoch, batches with 30 triplets are used to update the model. The margin in Equation 1 was set to 0.3, and the number of anchors is set to  $m = 2$ . We resize the images to  $256 \times 128 \times 3$  and apply Random Flipping and Random Erasing as data augmentation strategies during training.

### C. Comparison with the Prior Art

Tables I and II show results comparing the proposed method to the state of the art. The proposed method outperforms the other methods regarding mAP and Rank-1 in Market  $\rightarrow$  Duke by improving those values in 1.8 and 1.7 percentage points, respectively, and without using re-ranking. In the Duke  $\rightarrow$  Market scenario, we obtained a solid competitive performance by having values 0.1 percentage point lower only in Rank-1, also without re-ranking.

In turn, ABMT applied k-reciprocal encoding during training, which is more robust than Euclidean distance. However, it is more expensive to calculate as it is necessary to search for k-reciprocal neighbors of each feature vector in each iteration of the algorithm before clustering. In our case, we only apply the standard Euclidean distance during training, reducing the training time and complexity on adaptation, but still obtaining performance gains. Moreover, we have a single-term and single-hyper-parameter loss function, while ABMT depends on a loss with three terms and more hyper-parameters. They apply a teacher-student strategy to their training while we perform ensembling only for inference. Therefore, with a more direct pipeline and ensemble prediction, the proposed method has a Rank-1 only 0.1 percentage point lower in the Duke  $\rightarrow$  Market, while outperforming all methods in all other adaptation scenarios.

However, to benefit from the k-reciprocal encoding, we also apply it during inference to keep a simpler training process. This brings us the best performance in all scenarios in mAP and Rank-1 accuracy. In this case, the proposed method outperforms the methods in the prior art regarding mAP and Rank-1 in all adaptation scenarios.

Interestingly, the proposed method performs better under more difficult adaptation scenarios. We measure the difficulty of a scenario based on the number of different cameras it comprises. Market, Duke, and MSMT17 have 6, 8, and 15 cameras, respectively. Hence the most challenging adaptation scenario is from Market to MSMT17 (adaptation from 6 to 15 cameras). We adapt a model from a scenario with 6 cameras with all videos recorded in the same period of the day and the same season of the year to a target domain with 15 cameras (12 outdoors and 3 indoors) recorded at 3 different times on the day (morning, afternoon and noon) in 4 different days (each day on a different season of the year). Market  $\rightarrow$  MSMT17 is the most challenging adaptation and close to real-world conditions where we might have people recorded along the day and in different locations (indoors and outdoors). In this case, as shown in Table II, we obtained the highest performance even without relying upon re-ranking techniques. The proposed method outperforms the state-of-the-art by 1.5

and 2.1 percentage points in mAP and Rank-1, respectively, on Duke  $\rightarrow$  MSMT17, and by 2.2 and 4.2 percentage points on the most challenge scenario, Market  $\rightarrow$  MSMT17.

There are several reasons why our method performs better: we explicitly design a model to deal with the diversity of cameras and view points by creating a set of triplets based on the different cameras in a cluster, and we keep a more straightforward training with only one hyper-parameter in our loss function (triplet loss margin). Most works in the ReID literature optimize a loss function with many terms and hyper-parameters. They usually consider the Duke  $\rightarrow$  Market or the Market  $\rightarrow$  Duke scenarios (or both of them) to perform grid-searching over hyper-parameter values. Once they find the best values, they keep them unchanged for all adaptation setups.

In ABMT [16], the authors do not provide a clear explanation on how they define the hyper-parameter values for their loss function. However, they perform an ablation study over Duke  $\rightarrow$  Market and Market  $\rightarrow$  Duke scenarios, so their results might be biased to those specific setups, which gives them one of the best performances. However, when they keep the same values for different and more challenging scenarios, such as Market  $\rightarrow$  MSMT17 or Duke  $\rightarrow$  MSMT17, they obtain worse results than ours by a large margin. This shows that our method provides a better generalization capability brought by a simpler loss function and a more diverse training. It prevents us from choosing specific hyper-parameter values and be biased to a specific adaptation setup. Consequently, we achieve the best performances, especially in the most difficult scenarios.

#### D. Discussion

We aim to search for people in a camera system in an unsupervised way, so we must be robust to hyper-parameters that would require adjustments based on grid-searching using true label information, keeping the training process (and adaptation to a target domain) as simple as possible. If a pipeline is complex and too sensitive to hyper-parameters, it might be challenging to train and deploy it on a real investigation scenario, where we do not have prior knowledge about the people of interest. This complexity leads to sub-optimal performance. In this sense, algorithms should be less sensitive to hyper-parameter or ideally reduce them on adaptation stage. This assumption has already been pointed in the prior art. For instance, in [57], the authors claim that most prior work rely upon many hyper-parameters during the adaptation stage, which can help or hinder the model performance, depending on the value assigned to them and which adaptation scenario is considered.

SSKD[38] is an ensemble-based method leveraging three deep models in a co-teaching training regime with a four-term loss function with three hyper-parameters. One of the terms of their final loss function is a multi-similarity loss [58], with three extra hyper-parameters to train the model.

MEB-Net has complex training by relying upon a co-training technique with three deep neural networks in which each one learns with the others. Each of these three networks has its separate loss function with six terms, and their overall loss function is a weighted average of the individual loss functions from each model on the ensemble.

ABMT also leverages a teacher-student model where the teacher and student networks share the same architecture, increasing time and memory complexity during training. Moreover, they utilize a three-term loss function to optimize both models with three hyper-parameters controlling each term's contribution to the final loss. They update the teacher weights based on the exponential moving average (EMA) of the student weights, in order to avoid error label amplification on training. This also adds another parameter to control the inertia in the teacher weights' EMA. The authors do not perform an ablation study regarding the hyper-parameter value variation to assess their impact on final performance. In turn, we perform self-ensembling in our work by weighing each checkpoint's contribution directly considering the amount of target data used in the iteration. This prevents the need of additional hyper-parameters.

Based on these observations, our proposed model better captures the diversity of real cases, by considering a loss function with a single term and that is less sensitive to hyper-parameters (we must select only the margin  $\alpha$  value). In such setups, it is difficult to select hyper-parameter values correctly, as we might not know any information about the identities on the target domain. The self-ensembling also summarizes the whole training into a single model by using each checkpoint's confidence values over the target data, without using any hyper-parameter or human-defined value. Even adopting such a simpler formulation, we still obtain the state-of-the-art performance on the Market  $\rightarrow$  Duke scenario and competitive performance on the Duke  $\rightarrow$  Market scenario. ABMT and SSKD leverage an ensemble method during training time, making the training progress of one of the models dependent on the other model's answer. Each architecture in our work is trained in parallel without any co-teaching strategy. After self-ensembling, the joint contribution from different backbones is applied only on evaluation time, which avoids label propagation of noisy examples (e.g., potential outliers) but still takes advantage of the complementarity between them.

#### V. ABLATION STUDY

This section shows the contributions of each part of our pipeline in the final result. In each set of experiments, we change one of the parts and keep the others unchanged to check how it influences the final performance. If not explicitly mentioned, we consider ResNet50 as the backbone, OPTICS with hyper-parameter  $\xi = 0.05$ , and self-ensembling applied after training.

##### A. Impact of the Clustering Hyper-parameter

Although we have only one hyper-parameter in the loss function, we still need to define parameter  $\xi$  of the OPTICS clustering algorithm, which is a threshold in range  $[0, 1]$ . The closer  $\xi$  is to 0, the stronger is the criteria to define a cluster; that is, we might have many samples not assigned to any cluster, which leads to several detected outliers (if  $\xi = 0$ , all feature vectors are detected as outliers). In contrast, the closer  $\xi$  is to 1, the more relaxed is the criteria, and more samples are assigned to clusters (if  $\xi = 1$ , all feature vectors



TABLE I

RESULTS ON MARKET1501 TO DUKEMTMC-REID AND DUKEMTMC-REID TO MARKET1501 ADAPTATION SCENARIOS. WE REPORT MAP, RANK-1, RANK-5, AND RANK-10, COMPARING TO SEVERAL STATE-OF-ART METHODS. THE BEST RESULT IS SHOWN IN **BOLD**, THE SECOND IN UNDERLINE AND THE THIRD IN *italic*. WORKS WITH (\*) DO NOT PRE-TRAIN THE MODEL IN ANY SOURCE DATASET BEFORE ADAPTATION.

Method	reference	Duke → Market				Market → Duke			
		mAP	R1	R5	R10	mAP	R1	R5	R10
ATNet [19]	CVPR 2019	25.6	55.7	73.2	79.4	24.9	45.1	59.5	64.2
CamStyle [50]	TIP 2019	27.4	58.8	78.2	84.3	25.1	48.4	62.5	68.9
MAR [51]	CVPR 2019	40.0	67.7	81.9	-	48.0	67.1	79.8	-
PAUL [52]	CVPR 2019	40.1	68.5	82.4	87.4	53.2	72.0	82.7	86.0
ECN [31]	CVPR 2019	43.0	75.1	87.6	91.6	40.4	63.3	75.8	80.4
ISSDA-ReID [30]	CVPR 2019	63.1	81.3	92.4	95.2	54.1	72.8	82.9	85.9
PDA-Net [21]	ICCV 2019	47.6	75.2	86.3	90.2	45.1	63.2	77.0	82.5
CR-GAN [20]	ICCV 2019	54.0	77.7	89.7	92.7	48.6	68.9	80.2	84.7
PCB-PAST [10]	ICCV 2019	54.6	78.4	-	-	54.3	72.4	-	-
UCDA [26]	ICCV 2019	30.9	60.4	-	-	31.0	47.7	-	-
SSG [9]	ICCV 2019	58.3	80.0	90.0	92.4	53.4	73.0	80.6	83.2
CASCL [27]	ICCV 2019	35.5	65.4	80.6	86.2	37.8	59.3	73.2	77.8
SSL [53]*	CVPR 2020	37.8	71.7	83.8	87.4	28.6	52.5	63.5	68.9
UDAP [8]	PR 2020	53.7	75.8	89.5	93.2	49.0	68.4	80.1	83.5
MMCL [33]	CVPR 2020	60.4	84.4	92.8	95.0	51.4	72.4	82.9	85.0
ACT [37]	AAAI 2020	60.6	80.5	-	-	54.5	72.4	-	-
ECN-GPP [32]	TPAMI 2020	63.8	84.1	92.8	95.4	54.4	74.0	83.7	87.4
HCT [54]*	CVPR 2020	56.4	80.0	91.6	95.2	50.7	69.6	83.4	87.4
SNR [55]	CVPR 2020	61.7	82.8	-	-	58.1	76.3	-	-
AD-Cluster [11]	CVPR 2020	68.3	86.7	94.4	96.5	54.1	72.6	82.5	85.5
MMT [12]	ICLR 2020	71.2	87.7	94.9	96.9	65.1	78.0	88.8	92.5
CycAs [56]*	ECCV 2020	64.8	84.8	-	-	60.1	77.9	-	-
DG-Net++ [23]	ECCV 2020	61.7	82.1	90.2	92.7	63.8	78.9	87.8	90.4
MEB-Net [13]	ECCV 2020	76.0	89.9	96.0	97.5	66.1	79.6	88.3	92.2
Dual-Refinement [34]	arXiv 2020	78.0	90.9	96.4	97.7	67.7	82.1	90.1	92.5
SSKD [38]	arXiv 2020	78.7	91.7	<b>97.2</b>	<b>98.2</b>	67.2	80.2	<u>90.6</u>	<u>93.3</u>
ABMT [16]	WACV 2020	<u>80.4</u>	<u>93.0</u>	-	-	70.8	83.3	-	-
<b>Ours (w/o Re-Ranking)</b>	This Work	78.4	92.9	<u>96.9</u>	<u>97.8</u>	<u>72.6</u>	<u>85.0</u>	<u>92.1</u>	<b>93.9</b>
<b>Ours (w/ Re-Ranking)</b>	This Work	<b>88.0</b>	<b>93.8</b>	<i>96.4</i>	<i>97.4</i>	<b>82.7</b>	<b>87.2</b>	<b>92.5</b>	<b>93.9</b>

are grouped into a single cluster). In Figure 4, we show the impact of the threshold  $\xi$  for the Market → Duke and Duke → Market scenarios.

marginally better than  $\xi = 0.05$  for Market → Duke. Hence, we opt for  $\xi = 0.05$  in all adaptation scenarios.

### B. Impact of Curriculum Learning

In our pipeline, Stage 3 is responsible for cluster selection. After running the clustering algorithm, a feature vector can be an outlier, assigned to a cluster with only one camera or assigned to a cluster with two or more cameras. We argue that feature space cleaning is important for better adaptation, and that feature vectors in a cluster with at least two cameras are more reliable than ones assigned as outliers or to cluster with a single camera. Then, we consider the curriculum learning principle to select the most confident samples and learn in an easy-to-hard manner. To achieve this, we remove the outliers and the clusters with only one camera. To check the impact of this removal, we performed four experiments in which we alternate between keeping the outliers and the clusters with only one camera. The results are summarized in Table III.

We observe a performance gain on most of the metrics, especially on mAP and Rank-1, when we apply our cluster selection strategy. If we keep the outliers in the feature space (first and third rows in Table III), we face the most significant performance drop in both adaptation scenarios. It shows the importance of removing outliers after the clustering stage; otherwise, they can be considered in the creation of triplets, increasing the number of false negatives (for instance, selecting negative samples of the same real class) and, consequently,

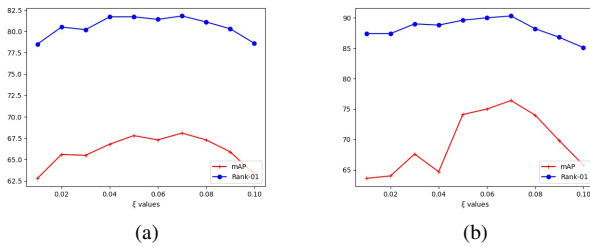


Fig. 4. Impact of clustering hyper-parameter  $\xi$ . Results on (a) Market → Duke and (b) Duke → Market.

We observe that the optimal value for  $\xi$  changes from an adaptation scenario to another, which is expected since we are dealing with different unseen target domains. In both cases, we have a Rank-1 curve more stable than mAP, showing that the parameter is less sensitive to retrieve the true positive image than calculate its confidence in the retrieving task. The best Rank-1 values are obtained for  $\xi$  between 0.04 and 0.08 considering both scenarios and, in the more challenging one (Market → Duke), it achieves the second-best value when  $\xi = 0.05$ , for both mAP and Rank-1. Although the best performance is achieved when  $\xi = 0.07$ , it relies on an unstable point in the graph of Duke → Market, and it is only

TABLE II

RESULTS ON MARKET1501 TO MSMT17 AND DUKEMTMCRE-ID TO MSMT17 ADAPTATION SCENARIOS. WE REPORT MAP, RANK-1, RANK-5, AND RANK-10, COMPARING TO SEVERAL STATE-OF-ART METHODS. THE BEST RESULT IS SHOWN IN **BOLD**, THE SECOND IN UNDERLINE AND THE THIRD IN *italic*. WORKS WITH (\*) DO NOT PRE-TRAIN THE MODEL IN ANY SOURCE DATASET BEFORE ADAPTATION.

Method	reference	Duke → MSMT17				Market → MSMT17			
		mAP	R1	R5	R10	mAP	R1	R5	R10
ECN [31]	CVPR 2019	10.2	30.2	41.5	46.8	8.5	25.3	36.3	42.1
SSG [9]	ICCV 2019	13.3	32.2	-	51.2	13.2	31.6	-	49.6
ECN-GPP [32]	TPAMI 2020	16.0	42.5	55.9	61.5	15.2	40.4	53.1	58.7
MMCL [33]	CVPR 2020	16.2	43.6	54.3	58.9	15.1	40.8	51.8	56.7
MMT [12]	ICLR 2020	23.3	50.1	63.9	69.8	22.9	49.2	63.1	68.8
CycAs [56]*	ECCV 2020	26.7	50.1	-	-	26.7	50.1	-	-
DG-Net++ [23]	ECCV 2020	22.1	48.8	60.9	65.9	22.1	48.4	60.9	66.1
Dual-Refinement [34]	arXiv 2020	26.9	55.0	68.4	73.2	25.1	53.3	66.1	71.5
SSKD [38]	arXiv 2020	26.0	53.8	66.6	72.0	23.8	49.6	63.1	68.8
ABMT [16]	WACV 2020	33.0	61.8	-	-	27.8	55.5	-	-
SpCL [59]	NeurIPS 2020	-	-	-	-	31.0	58.1	69.6	74.1
<b>Ours (w/o Re-Ranking)</b>	This Work	<u>34.5</u>	<u>63.9</u>	<u>75.3</u>	<u>79.6</u>	<u>33.2</u>	<u>62.3</u>	<u>74.1</u>	<u>78.5</u>
<b>Ours (w/ Re-Ranking)</b>	This Work	<b>46.6</b>	<b>69.6</b>	<b>77.1</b>	<b>80.4</b>	<b>45.2</b>	<b>68.1</b>	<b>76.0</b>	<b>79.2</b>

TABLE III

IMPACT OF CURRICULUM LEARNING, WHEN CONSIDERING DIFFERENT CLUSTER SELECTION CRITERIA. WE TESTED OUR METHOD WITH AND WITHOUT OUTLIERS AND WITH AND WITHOUT CLUSTERS WITH ONLY ONE CAMERA IN THE FEATURE SPACE. ALL EXPERIMENTS CONSIDER RESNET50 AS THE BACKBONE WITH SELF-ENSEMBLING APPLIED AFTER TRAINING.

w/o outliers	w/o cluster with one camera	Duke → Market				Market → Duke			
		mAP	R1	R5	R10	mAP	R1	R5	R10
-	-	50.9	79.2	89.5	92.8	32.7	56.7	68.5	72.9
✓	-	72.4	89.5	95.2	96.7	66.8	81.1	<b>90.2</b>	92.4
-	✓	49.1	79.8	89.5	92.6	32.7	57.2	68.4	72.3
✓	✓	<b>74.1</b>	<b>89.6</b>	<b>95.3</b>	<b>97.1</b>	<b>67.8</b>	<b>81.7</b>	90.0	<b>92.6</b>

hindering the performance. We see a lower performance drop by keeping clusters with only one camera but without outliers (second row), indicating that those clusters do not hinder the performance much but might consider noisy samples for model updating. It is more evident when we verify that the most gains were over mAP and lower gains over Rank-1 in the last row. This demonstrates that if we keep one-camera clusters, the model can still retrieve most of the gallery's correct images but with lower confidence. Hence, the cluster selection criteria effectively improves our model generalization and we apply it in all adaptation scenarios.

With this strategy, we observe that the percentage of feature vectors from the target domain kept in the feature space increases during the adaptation, as shown in Figures 5c and 6c. In fact, reliability, mAP and Rank-1 increase during training (Figures 5 and 6), which means that the model becomes more robust in the target domain as more iterations are performed. This demonstrates the curriculum learning importance, where easier examples at the beginning of the training (images whose feature vectors are assigned to clusters with at least two cameras in early iterations) are used to give an initial knowledge about the unseen target domain and allow the model to increase its performance gradually.

### C. Impact of self-ensembling

To check the contribution of our proposed self-ensembling method explained in Section III-E, we take the best checkpoint of our model during adaptation in both scenarios, considering all backbones, and compare it with the self-ensembled model.

Note that we select the best model only for reference. In practice, we do not know the best checkpoint during training since we do not have any identity-label information. Our goal here is merely to show that our self-ensembling method leads to a final model that outperforms any checkpoint individually. Even if we do not have any label information to choose the best one during training, the self-ensembling can summarize the whole training process in a final model, which is better than all checkpoints. Table IV shows these results.

Our proposed self-ensembling method can improve the target domain's discrimination capacity by summarizing the whole training during adaptation. The method outperforms the best models in mAP by 2.0, 4.5 and 4.3 percentage points in Duke → Market for ResNet50, OSNet and DenseNet121, respectively. Similarly, for Market → Duke we achieve an improvement of 1.6, 2.2 and 3.3 percentage points in mAP for ResNet50, OSNet and DenseNet121, respectively. We can also observe gains for all backbones in both scenarios considering Rank-1. Therefore, our proposed self-ensembling strategy increases the number of correct examples retrieved from the gallery and its confidence. It shows that different checkpoints trained with different percentages of the data from the target domain have complementary information. Besides, as the self-ensembling is performed at the parameter level, without human supervision and considering each checkpoint's confidence, it reduces the memory footprint by eliminating all unnecessary checkpoints and keeping only the self-ensembled final model.

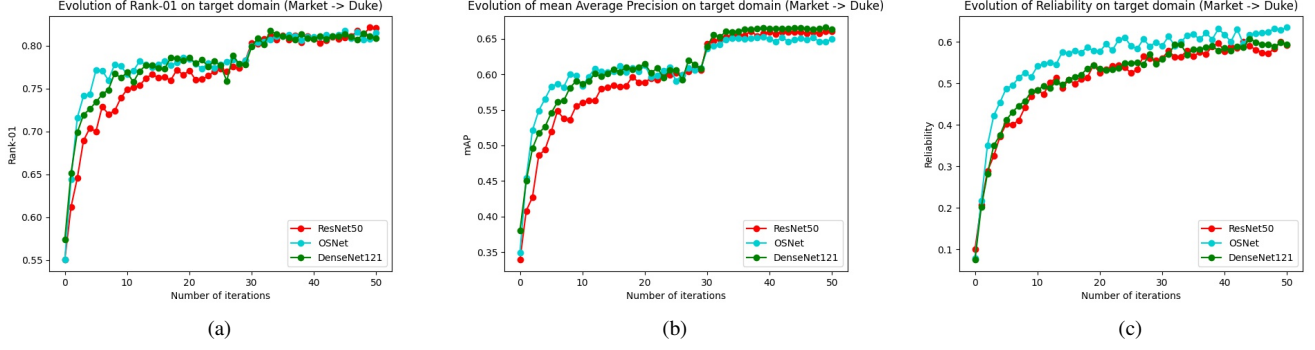


Fig. 5. Progress on Rank-1, mean Average Precision and Reliability on target dataset on Market1501 to DukeMTMC-ReID scenario.

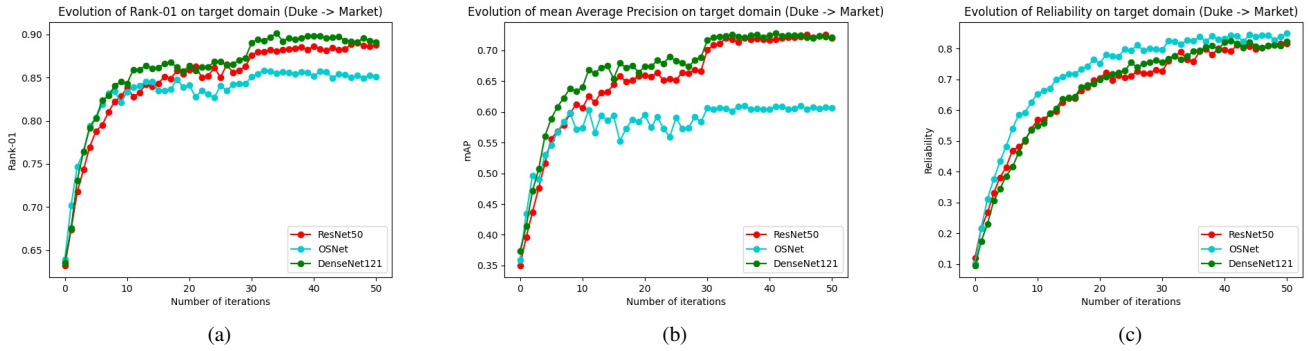


Fig. 6. Progress on Rank-1, mean Average Precision and Reliability on target dataset on DukeMTMC-ReID to Market1501 scenario.

TABLE IV

IMPACT OF SELF-ENSEMBLING. WE CONSIDER A WEIGHTED AVERAGE OF THE PARAMETERS OF THE BACKBONE IN DIFFERENT MOMENTS OF THE ADAPTATION. “BEST” REFERS TO RESULTS OBTAINED WITH THE CHECKPOINT WITH HIGHEST RANK-1 DURING ADAPTATION. “FUSION” IS THE FINAL MODEL CREATED THROUGH THE PROPOSED SELF-ENSEMBLING METHOD. THE BEST RESULTS ARE IN **BOLD**.

	Duke → Market				Market → Duke			
	mAP	R1	R5	R10	mAP	R1	R5	R10
ResNet (Best)	72.1	89.0	<b>95.5</b>	<b>97.1</b>	66.2	81.5	89.5	92.2
ResNet (Fusion)	<b>74.1</b>	<b>89.6</b>	95.3	<b>97.1</b>	<b>67.8</b>	<b>81.7</b>	<b>90.0</b>	<b>92.6</b>
OSNet (Best)	60.7	85.8	93.5	95.9	65.1	81.7	90.3	92.1
OSNet (Fusion)	<b>65.2</b>	<b>87.7</b>	<b>94.8</b>	<b>96.6</b>	<b>67.3</b>	<b>82.1</b>	<b>90.5</b>	<b>92.4</b>
DenseNet (Best)	72.6	90.1	95.6	97.1	66.0	81.7	90.1	92.4
DenseNet (Fusion)	<b>76.9</b>	<b>92.0</b>	<b>96.5</b>	<b>97.7</b>	<b>69.3</b>	<b>83.4</b>	<b>91.3</b>	<b>93.0</b>

#### D. Impact of Ensemble-based prediction

To increase the model’s discriminability, we combine distances computed by all considered architectures (Equation 3) for the final inference. Results are shown in Table V.

The ensemble model outperforms the individual models by 3.3, 5.2 and 0.9 percentage points regarding Rank-1, on Duke → Market, for ResNet50, OSNet and DenseNet, respectively. The same can be observed for Market → Duke, in which Rank-1 is improved by 3.3, 2.9 and 1.6 percentage points for ResNet50, OSNet and DenseNet121, respectively. Results for all the other metrics also increase for both adaptation scenarios. Therefore, we can effectively combine knowledge encoded in models with different architectures. By performing it only for inference, we keep a simpler training process and still can take advantage of the ensemble knowledge from different backbones.

#### VI. CONCLUSIONS AND FUTURE WORK

In this work, we tackle the problem of cross-domain Person Re-Identification (ReID) with non-overlapping cameras, especially targeting forensic scenarios with fast deployment requirements. We propose an Unsupervised Domain Adaptation (UDA) pipeline, with three novel techniques: (1) cross-camera triplet creation aiming at increasing diversity during training; (2) self-ensembling, to summarize complementary information acquired at different iterations during training; and (3) an ensemble-based prediction technique to take advantage of the complementarity between different trained backbones.

Our cross-camera triplet creation technique increases the model’s invariance to different points-of-view and types of cameras in the target domain and the regularization of the model, allowing the use of a single-term and single-hyperparameter triplet loss function. Moreover, we showed the

TABLE V  
IMPACT OF ENSEMBLING. PERFORMANCE WITH AND WITHOUT MODEL ENSEMBLE DURING INFERENCE. BEST VALUES ARE IN **BOLD**.

	Duke → Market				Market → Duke			
	mAP	R1	R5	R10	mAP	R1	R5	R10
ResNet (Fusion)	74.1	89.6	95.3	97.1	67.8	81.7	90.0	92.6
OSNet (Fusion)	65.2	87.7	94.8	96.6	67.3	82.1	90.5	92.4
DenseNet (Fusion)	76.9	92.0	96.5	97.7	69.3	83.4	91.3	93.0
Ensembled model	<b>78.4</b>	<b>92.9</b>	<b>96.9</b>	<b>97.8</b>	<b>72.6</b>	<b>85.0</b>	<b>92.1</b>	<b>93.9</b>

importance of having this more straightforward loss function, as it is less biased towards specific scenarios and helps us achieve state-of-art results in the most complex adaptation scenarios, surpassing prior art by a large margin.

The self-ensembling technique helps us increase the final performance by aggregating information from different checkpoints throughout the training process, without any human or label supervision. This is inspired by the reliability measurement, which shows us that our models learn from more reliable data as more iterations are performed. This is done in an easy-to-hard manner to increase model confidence gradually.

Finally, our last ensemble technique takes advantage of the complementarity between different backbones, enabling us to achieve state-of-the-art results without adding complexity to the training, differently from the mutual-learning strategies used in recent methods [13], [38], [16]. It is important to note that both ensembling strategies are done after training to generate a final model and a final prediction.

As the training process is simple compared to other state-of-the-art methods and because we do not need information on the target domain's identities, our work is easily extendable to other adaptation scenarios and deployed in actual investigations and other forensic contexts.

A key aspect of our method also shared with other recent methods in literature [27], [11], [32], is that it requires information about the camera used to acquire each sample. That is, we suppose we know, *a priori*, the device that captured each image. This information does not need to be the specific type of camera but, at least, information about different camera models. Without this information, our model could face suboptimal performance, as it would not be able to take advantage of the diversity introduced by the cross-camera triplets. To address this drawback, we aim to extend this work by incorporating techniques for automatic camera attribution [60], [61], allowing the identification of the camera used to acquire an image or identifying whether the same camera acquired a pair of images.

Regarding the clustering process, our method requires that all selected samples are considered during this phase, which demands pairwise distance calculation between all feature vectors. This approach may introduce higher processing times to the pipeline. In this sense, we also aim to extend our method to scale to very large datasets by introducing online deep clustering and self-supervised techniques directly in the pipeline.

Another possible extension of our pipeline can be its application to general object re-identification, such as vehicle ReID, to mine critical objects of interest in an investigation. Together with Person ReID, this could enable a joint analysis

by matching mined identities and objects to finally propose relations between them during an event's analysis.

#### ACKNOWLEDGMENT

We thank the financial support of the São Paulo Research Foundation (FAPESP) through the grants DéjàVu #2017/12646-3 and #2019/15825-1.

#### REFERENCES

- [1] R. Padilha, C. M. Rodrigues, F. A. Andaló, G. Bertocco, Z. Dias, and A. Rocha, "Forensic event analysis: From seemingly unrelated data to understanding," *IEEE Security and Privacy*, vol. 18, no. 6, pp. 23–32, 2020.
- [2] X. Qian, Y. Fu, Y.-G. Jiang, T. Xiang, and X. Xue, "Multi-scale deep learning architectures for person re-identification," in *International Conference on Computer Vision*, 2017, pp. 5399–5408.
- [3] Y. Sun, L. Zheng, Y. Yang, Q. Tian, and S. Wang, "Beyond part models: Person retrieval with refined part pooling (and a strong convolutional baseline)," in *European Conference on Computer Vision*, 2018, pp. 480–496.
- [4] K. Zhou, Y. Yang, A. Cavallaro, and T. Xiang, "Omni-scale feature learning for person re-identification," in *International Conference on Computer Vision*, 2019, pp. 3702–3712.
- [5] X. Chen, C. Fu, Y. Zhao, F. Zheng, J. Song, R. Ji, and Y. Yang, "Saliency-guided cascaded suppression network for person re-identification," in *IEEE Conference on Computer Vision and Pattern Recognition*, 2020, pp. 3300–3310.
- [6] C. Liu, X. Chang, and Y.-D. Shen, "Unity style transfer for person re-identification," in *IEEE Conference on Computer Vision and Pattern Recognition*, 2020, pp. 6887–6896.
- [7] H. Fan, L. Zheng, C. Yan, and Y. Yang, "Unsupervised person re-identification: Clustering and fine-tuning," *ACM Transactions on Multimedia Computing, Communications, and Applications*, vol. 14, no. 4, pp. 1–18, 2018.
- [8] L. Song, C. Wang, L. Zhang, B. Du, Q. Zhang, C. Huang, and X. Wang, "Unsupervised domain adaptive re-identification: Theory and practice," *Pattern Recognition*, vol. 102, p. 107173, 2020.
- [9] Y. Fu, Y. Wei, G. Wang, Y. Zhou, H. Shi, and T. S. Huang, "Self-similarity grouping: A simple unsupervised cross domain adaptation approach for person re-identification," in *International Conference on Computer Vision*, 2019, pp. 6112–6121.
- [10] X. Zhang, J. Cao, C. Shen, and M. You, "Self-training with progressive augmentation for unsupervised cross-domain person re-identification," in *International Conference on Computer Vision*, 2019, pp. 8222–8231.
- [11] Y. Zhai, S. Lu, Q. Ye, X. Shan, J. Chen, R. Ji, and Y. Tian, "Ad-cluster: Augmented discriminative clustering for domain adaptive person re-identification," in *IEEE Conference on Computer Vision and Pattern Recognition*, 2020, pp. 9021–9030.
- [12] Y. Ge, D. Chen, and H. Li, "Mutual mean-teaching: Pseudo label refinery for unsupervised domain adaptation on person re-identification," *arXiv preprint*, vol. arXiv:2001.01526, 2020.
- [13] Y. Zhai, Q. Ye, S. Lu, M. Jia, R. Ji, and Y. Tian, "Multiple expert brainstorming for domain adaptive person re-identification," *arXiv preprint*, vol. arXiv:2007.01546, 2020.
- [14] G. Hinton, O. Vinyals, and J. Dean, "Distilling the knowledge in a neural network," *arXiv preprint*, vol. arXiv:1503.02531, 2015.
- [15] B. Han, Q. Yao, X. Yu, G. Niu, M. Xu, W. Hu, I. Tsang, and M. Sugiyama, "Co-teaching: Robust training of deep neural networks with extremely noisy labels," in *Advances in Neural Information Processing Systems*, 2018, pp. 8527–8537.

- [16] H. Chen, B. Lagadec, and F. Bremond, "Enhancing diversity in teacher-student networks via asymmetric branches for unsupervised person re-identification," in *IEEE Winter Conference on Applications of Computer Vision*, 2020, pp. 1–10.
- [17] W. Deng, L. Zheng, Q. Ye, G. Kang, Y. Yang, and J. Jiao, "Image-image domain adaptation with preserved self-similarity and domain-dissimilarity for person re-identification," in *IEEE Conference on Computer Vision and Pattern Recognition*, 2018, pp. 994–1003.
- [18] L. Wei, S. Zhang, W. Gao, and Q. Tian, "Person transfer GAN to bridge domain gap for person re-identification," in *IEEE Conference on Computer Vision and Pattern Recognition*, 2018, pp. 79–88.
- [19] J. Liu, Z.-J. Zha, D. Chen, R. Hong, and M. Wang, "Adaptive transfer network for cross-domain person re-identification," in *IEEE Conference on Computer Vision and Pattern Recognition*, 2019, pp. 7202–7211.
- [20] Y. Chen, X. Zhu, and S. Gong, "Instance-guided context rendering for cross-domain person re-identification," in *International Conference on Computer Vision*, 2019, pp. 232–242.
- [21] Y.-J. Li, C.-S. Lin, Y.-B. Lin, and Y.-C. F. Wang, "Cross-dataset person re-identification via unsupervised pose disentanglement and adaptation," in *International Conference on Computer Vision*, 2019, pp. 7919–7929.
- [22] Z. Zhong, L. Zheng, S. Li, and Y. Yang, "Generalizing a person retrieval model hetero-and homogeneously," in *European Conference on Computer Vision*, 2018, pp. 172–188.
- [23] Y. Zou, X. Yang, Z. Yu, B. Kumar, and J. Kautz, "Joint disentangling and adaptation for cross-domain person re-identification," *arXiv preprint*, vol. arXiv:2007.10315, 2020.
- [24] J. Wang, X. Zhu, S. Gong, and W. Li, "Transferable joint attribute-identity deep learning for unsupervised person re-identification," in *IEEE Conference on Computer Vision and Pattern Recognition*, 2018, pp. 2275–2284.
- [25] S. Lin, H. Li, C.-T. Li, and A. C. Kot, "Multi-task mid-level feature alignment network for unsupervised cross-dataset person re-identification," *arXiv preprint*, vol. arXiv:1807.01440, 2018.
- [26] L. Qi, L. Wang, J. Huo, L. Zhou, Y. Shi, and Y. Gao, "A novel unsupervised camera-aware domain adaptation framework for person re-identification," in *International Conference on Computer Vision*, 2019, pp. 8080–8089.
- [27] A. Wu, W.-S. Zheng, and J.-H. Lai, "Unsupervised person re-identification by camera-aware similarity consistency learning," in *International Conference on Computer Vision*, 2019, pp. 6922–6931.
- [28] S. Lloyd, "Least squares quantization in PCM," *IEEE Transactions on Information Theory*, vol. 28, no. 2, pp. 129–137, 1982.
- [29] M. Ester, H.-P. Kriegel, J. Sander, and X. Xu, "A density-based algorithm for discovering clusters in large spatial databases with noise," in *International Conference on Knowledge Discovery and Data Mining*, 1996, pp. 226–231.
- [30] H. Tang, Y. Zhao, and H. Lu, "Unsupervised person re-identification with iterative self-supervised domain adaptation," in *IEEE Conference on Computer Vision and Pattern Recognition Workshops*, 2019, pp. 1536–1543.
- [31] Z. Zhong, L. Zheng, Z. Luo, S. Li, and Y. Yang, "Invariance matters: Exemplar memory for domain adaptive person re-identification," in *IEEE Conference on Computer Vision and Pattern Recognition*, 2019, pp. 598–607.
- [32] —, "Learning to adapt invariance in memory for person re-identification," *IEEE Transactions on Pattern Analysis and Machine Intelligence*, pp. 1–1, 2020.
- [33] D. Wang and S. Zhang, "Unsupervised person re-identification via multi-label classification," in *IEEE Conference on Computer Vision and Pattern Recognition*, 2020, pp. 10981–10990.
- [34] Y. Dai, J. Liu, Y. Bai, Z. Tong, and L.-Y. Duan, "Dual-refinement: Joint label and feature refinement for unsupervised domain adaptive person re-identification," *arXiv preprint*, vol. arXiv:2012.13689, 2020.
- [35] R. J. Campello, D. Moulavi, and J. Sander, "Density-based clustering based on hierarchical density estimates," in *Pacific-Asia Conference on Knowledge Discovery and Data Mining*, 2013, pp. 160–172.
- [36] M. Ankerst, M. M. Breunig, H.-P. Kriegel, and J. Sander, "OPTICS: ordering points to identify the clustering structure," *ACM SIGMOD Record*, vol. 28, no. 2, pp. 49–60, 1999.
- [37] F. Yang, K. Li, Z. Zhong, Z. Luo, X. Sun, H. Cheng, X. Guo, F. Huang, R. Ji, and S. Li, "Asymmetric co-teaching for unsupervised cross-domain person re-identification," in *AAAI Conference on Artificial Intelligence*, 2020, pp. 12597–12604.
- [38] J. Yin, J. Qiu, S. Zhang, Z. Ma, and J. Guo, "SSKD: Self-supervised knowledge distillation for cross domain adaptive person re-identification," *arXiv preprint*, vol. arXiv:2009.05972, 2020.
- [39] L. Jiang, D. Meng, S.-I. Yu, Z. Lan, S. Shan, and A. Hauptmann, "Self-paced learning with diversity," *Advances in Neural Information Processing Systems*, vol. 27, pp. 2078–2086, 2014.
- [40] F. Schroff, D. Kalenichenko, and J. Philbin, "FaceNet: A unified embedding for face recognition and clustering," in *IEEE Conference on Computer Vision and Pattern Recognition*, 2015, pp. 815–823.
- [41] Z. Zhong, L. Zheng, D. Cao, and S. Li, "Re-ranking person re-identification with k-reciprocal encoding," in *IEEE Conference on Computer Vision and Pattern Recognition*, 2017, pp. 1318–1327.
- [42] L. Zheng, L. Shen, L. Tian, S. Wang, J. Wang, and Q. Tian, "Scalable person re-identification: A benchmark," in *International Conference on Computer Vision*, 2015, pp. 1116–1124.
- [43] E. Ristani, F. Solera, R. Zou, R. Cucchiara, and C. Tomasi, "Performance measures and a data set for multi-target, multi-camera tracking," in *European Conference on Computer Vision*, 2016, pp. 17–35.
- [44] K. He, X. Zhang, S. Ren, and J. Sun, "Deep residual learning for image recognition," in *IEEE Conference on Computer Vision and Pattern Recognition*, 2016, pp. 770–778.
- [45] G. Huang, Z. Liu, L. Van Der Maaten, and K. Q. Weinberger, "Densely connected convolutional networks," in *IEEE Conference on Computer Vision and Pattern Recognition*, 2017, pp. 4700–4708.
- [46] J. Deng, W. Dong, R. Socher, L.-J. Li, K. Li, and L. Fei-Fei, "Imagenet: A large-scale hierarchical image database," in *IEEE Conference on Computer Vision and Pattern Recognition*, 2009, pp. 248–255.
- [47] K. Zhou and T. Xiang, "Torchreid: A library for deep learning person re-identification in Pytorch," *arXiv preprint*, vol. arXiv:1910.10093, 2019.
- [48] A. Paszke, S. Gross, F. Massa, A. Lerer, J. Bradbury, G. Chanan, T. Killeen, Z. Lin, N. Gimelshein, L. Antiga, A. Desmaison, A. Kopf, E. Yang, Z. DeVito, M. Raison, A. Tejani, S. Chilamkurthy, B. Steiner, L. Fang, J. Bai, and S. Chintala, "PyTorch: An imperative style, high-performance deep learning library," in *Advances in Neural Information Processing Systems*, 2019, pp. 8024–8035.
- [49] D. P. Kingma and J. Ba, "Adam: A method for stochastic optimization," *arXiv preprint*, vol. arXiv:1412.6980, 2014.
- [50] Z. Zhong, L. Zheng, Z. Zheng, S. Li, and Y. Yang, "Camstyle: A novel data augmentation method for person re-identification," *IEEE Transactions on Image Processing*, vol. 28, no. 3, pp. 1176–1190, 2018.
- [51] H.-X. Yu, W.-S. Zheng, A. Wu, X. Guo, S. Gong, and J.-H. Lai, "Unsupervised person re-identification by soft multilabel learning," in *IEEE Conference on Computer Vision and Pattern Recognition*, 2019, pp. 2148–2157.
- [52] Q. Yang, H.-X. Yu, A. Wu, and W.-S. Zheng, "Patch-based discriminative feature learning for unsupervised person re-identification," in *IEEE Conference on Computer Vision and Pattern Recognition*, 2019, pp. 3633–3642.
- [53] Y. Lin, L. Xie, Y. Wu, C. Yan, and Q. Tian, "Unsupervised person re-identification via softened similarity learning," in *IEEE Conference on Computer Vision and Pattern Recognition*, 2020, pp. 3390–3399.
- [54] K. Zeng, M. Ning, Y. Wang, and Y. Guo, "Hierarchical clustering with hard-batch triplet loss for person re-identification," in *IEEE Conference on Computer Vision and Pattern Recognition*, 2020, pp. 13657–13665.
- [55] X. Jin, C. Lan, W. Zeng, Z. Chen, and L. Zhang, "Style normalization and restitution for generalizable person re-identification," in *IEEE Conference on Computer Vision and Pattern Recognition*, 2020, pp. 3143–3152.
- [56] Z. Wang, J. Zhang, L. Zheng, Y. Liu, Y. Sun, Y. Li, and S. Wang, "CycAs: Self-supervised cycle association for learning re-identifiable descriptions," *arXiv preprint*, vol. arXiv:2007.07577, 2020.
- [57] F. Dubourvieux, R. Audigier, A. Loesch, S. Ainouz, and S. Canu, "Unsupervised domain adaptation for person re-identification through source-guided pseudo-labeling," *arXiv preprint*, vol. arXiv:2009.09445, 2020.
- [58] X. Wang, X. Han, W. Huang, D. Dong, and M. R. Scott, "Multi-similarity loss with general pair weighting for deep metric learning," in *IEEE Conference on Computer Vision and Pattern Recognition*, 2019, pp. 5022–5030.
- [59] Y. Ge, D. Chen, F. Zhu, R. Zhao, and H. Li, "Self-paced contrastive learning with hybrid memory for domain adaptive object re-id," *arXiv preprint*, vol. arXiv:2006.02713, 2020.
- [60] F. d. O. Costa, E. Silva, M. Eckmann, W. J. Scheirer, and A. Rocha, "Open set source camera attribution and device linking," *Pattern Recognition Letters*, vol. 39, pp. 92–101, 2014.
- [61] J. Bernacki, "A survey on digital camera identification methods," *Forensic Science International: Digital Investigation*, vol. 34, p. 300983, 2020.